IEEE Access
Multidisciplinary | Rapid Review | Open Access Journal

Received August 9, 2021, accepted August 16, 2021, date of publication August 24, 2021, date of current version September 3, 2021.

Digital Object Identifier 10.1109/ACCESS.2021.3107674

Multi-Tier Variable Height UAV Networks: User Coverage and Throughput Optimization

MUHAMMAD NAFEES, (Member, IEEE), JOHN THOMPSON, (Fellow, IEEE), AND MAJID SAFARI, (Senior Member, IEEE)
School of Engineering, Institute for Digital Communications, The University of Edinburgh, Edinburgh EH9 3JL, U.K.

Corresponding author: Muhammad Nafees (m.nafees@ed.ac.uk)

The work of Majid Safari was supported by the Engineering and Physical Sciences Research Council (EPSRC) through the Terabit Bidirectional Multi-User Optical Wireless System (TOWS) for 6G LiFi under Program EP/S016570/1.

ABSTRACT Unmanned aerial vehicles (UAVs) are increasingly considered to act as base stations (BSs) for the future wireless networks. Some of the crucial UAV-assisted network design challenges are the network coverage, throughput, and energy efficiency. Therefore, fast, low-complexity, and efficient UAV placement and resource allocation strategies are imperative. This paper presents a novel variable height multi-UAV deployment strategy to exploit the 3D flexibility of UAVs as BSs. We propose a multi-tier variable height UAV-based network deployment and compare its performance with the state-of-the-art equal height deployment. Height optimization is performed to deliver energy efficiency and throughput maximization for each cell. The results show that our proposed method is more energy-efficient in a multi-cell UAV network than the most widely used height optimization method in the literature. In UAV networks, users at the cell edges can receive very poor signal-to-interference-plus-noise ratio (SINR) levels due to interfering UAVs. To cope with this problem, we adopt a fractional frequency reuse (FFR) scheme to compensate low SINR levels. We optimize the SINR threshold corresponding to each cell to maximize their spectral efficiency (SE), thereby improving the network's area spectral efficiency (ASE). The numerical results show that the proposed deployments provide significant gains in coverage density, SINR coverage probability, rate coverage, and ASE compared to equal height benchmark scheme. As the number of UAVs increases, the number of tiers need to increase to preserve the rate coverage of the network. Moreover, the performance of the proposed variable height model is expected to converge to that of equal height cellular design for a large number of UAVs.

INDEX TERMS Unmanned aerial vehicles (UAVs), signal-to-interference-plus-noise ratio (SINR), fractional frequency reuse (FFR), area spectral efficiency (ASE), reinforcement learning (RL).

I. INTRODUCTION

The use of unmanned aerial vehicles (UAVs) has been extremely appealing for improving wireless communication systems. One of the primary reasons for the growing popularity of UAVs is their interoperability and ability to adapt to a variety of situations for both civilian and military use [1], [2]. In comparison to terrestrial mobile networks, UAV-assisted wireless networks have some significant advantages. For instance, these networks can be rapidly deployed for on-demand and emergency communications such as in disaster-hit areas when conventional base stations (BSs) are damaged by a disaster or in hotspot areas. Furthermore, UAVs offer an inherent advantage in terms of a higher probability for a line-of-sight (LoS) connection due to the high altitude compared to the ground network infrastructure, which can greatly improve the quality-of-service (QoS) of the network. Moreover, these networks are adaptive in terms of various parameters (i.e., height, location, transmit power, etc.) and the mobility of UAVs offers an additional degree of freedom for flexible deployments, and thus, UAVs can offer fast, on-demand wireless communications [3]. By contrast, most of these advantages are not offered by the terrestrial BSs due to fixed ground-based deployments.

UAV-assisted communication use cases can be classified into four main areas, namely relaying, information

The associate editor coordinating the review of this manuscript and approving it for publication was Kathiravan Srinivasan.

broadcasting, data collection, and deployment optimization [4]. Deployment scenarios have attained a lot of attraction for providing wireless coverage (e.g., [5]–[7]). Due to the limited resource capability of a single UAV network, a multi-UAV network is efficient for various missions [8]. The use of UAVs is being practically realized now in the telecommunications industry. For example, Qualcomm has tested the operability of UAVs for the long term evolution (LTE) and fifth-generation (5G) cellular applications [9]. Ericsson performed trials for 5G interference management with drones, previously they proposed connected drone testing as a fourth-generation (4G) network solution [10]. As a result, 5G and beyond 5G (B5G) wireless networks will be able to use UAVs as an essential part of the next generation of mobile networks, and UAVs are also envisioned to work as a single system [11].

A. RELATED WORK AND CONTRIBUTION

How to optimize the network's coverage and throughput for a given number of UAVs is a practical and interesting problem. This wireless coverage problem using UAVs is studied by Al-Hourani *et al*. [12] by utilizing a new air-to-ground (AtG) channel model. The authors also determined an optimal UAV height for maximum coverage of ground users. An iterative algorithm is developed in [13] using block coordinate descent and successive convex optimization to maximize the aggregate statistical-QoS-guaranteed throughput of all users by optimizing the UAV's 3D position, power, and bandwidth allocation with users' different QoS requirements. Another network reconstruction problem is investigated in [14], assuming that ad-hoc networks are impaired in the aftermath of a disaster. The objective is to repair the network by adding aerial wireless links with the help of UAVs.

Singh *et al.* [15] determined optimal and sub-optimal 3D positioning of UAVs to maximize the network throughput. Two strategies for UAV selection are proposed: harmonic mean and best downlink signal-to-noise ratio (SNR). In [16], multi-UAV deployment is considered to provide some design guidelines for coverage performance in the presence of interference by varying the UAV height in different working environments to obtain best coverage configuration for a given set of UAVs. An optimal 3D deployment of a heterogeneous set of UAVs is proposed by Namvar *et al*. [17] to maximize wireless coverage in a rectangular coverage area. The proposed algorithm discovers an optimal subset of the available UAVs and their 3D placement to deliver maximum network coverage.

Most of the existing literature considered UAV-assisted networks based on the assumptions of a guaranteed LoS connection (e.g., [18], [19]). Also, the use of directional antennas is considered whereas effect of interference is often neglected [20]. A similar optimal UAV deployment method in a square region is proposed in [7], assuming all links in the region were LoS and directional antennas are used for coverage maximization. Another optimal UAV location problem for the data rate maximization is considered by Li *et al.* [21] assuming a stationary UAV and a ground user. Some research studies have included interference considerations in their analysis. For example, a multi-UAV interference coordination technique is proposed in [22] with joint trajectory and power control for maximizing the aggregate total rate for a given flight interval. Lyu *et al*. [23] presented an interference-aware deployment policy for UAV-relays to compensate for congestion and to reduce the outage probability.

Machine learning has recently received a lot of attention in the area of UAV networks. For instance, a novel Q-learning-based topology-aware routing protocol is proposed in [8] to deliver reliable communications for flying ad hoc networks. Arani *et al.* [24] proposed a space-terrestrial network using UAVs and satellites to solve the backhaul connectivity problem of UAVs by using a reinforcement learning (RL) framework to jointly optimize the 3D trajectory of UAVs, resource management, and user associations. A deep-RL based method is proposed in [25] to maximize the UAV's energy efficiency, considering both aerodynamic and communication energy while ensuring the communication requirements for each user and the backhaul link between the UAV and the terrestrial BS.

For multi-UAV network deployments, equal-size circle packing has been exploited for a variety of applications. Mozaffari *et al.* [5] first proposed to employ equal-size circle packing for the UAV deployments. As a function of UAV height and directional antenna gain, a coverage probability expression is also derived. A simple circular trajectory is used in [26] to propose a trajectory initialization scheme using equal-size circle packing for maximizing the minimum average user rate. In a related study, an optimal UAV placement algorithm is proposed to deploy UAVs using the smallest enclosed circle problem for maximizing the users covered with minimum transmit power [27]. Shakhatreh *et al.* [28] maximized indoor wireless coverage using equal-size circle packing in rectangular and square coverage regions by covering one and then two sides of the same building. The authors extended the study in [29] to cover a more demanding QoS environment. A circle packing based decision mechanism in a square region is also proposed by Gao *et al.* [30] for an AtG collaborative vehicular network to maximize the coverage while minimizing the energy consumed by the small drone cells. The work in [20] exploited three equal-size circles to compare and contrast with hexagon packing to exhibit an interplay among the radius, height and beamwidth of practical UAV systems.

In emergency and hotspot circumstances, the need for a low-complexity and efficient deployment strategy motivates us to develop a systematic and rigorous UAV deployment technique. The method should not only allow UAVs to be deployed quickly but also enables simple UAV failure handling. In this paper, we propose UAV-assisted network deployments by exploiting the variable-size circle packing using a tractable multi-tier approach to deploy a number of UAVs in a circular coverage area. We compare the performance of the proposed deployments with equal-size circle

packing based UAV networks. The main contributions of this paper are summarized as follows.

- We propose a UAV-based cellular network design using multi-tier variable-size circle packing to maximize network coverage. We first introduce the two-tier UAV design and then show that there is a tractable way to extend the two-tier model to multiple tiers where resource availability of the UAVs is taken into account.
- We provide a new method to optimize the height of UAVs to maximize the average throughput of the cells using an RL technique. Our approach provides higher signal-to-interference-plus-noise ratio (SINR) levels and lower flying heights than the state of the art UAV height optimization method [12], [16], [17], [31].
- We develop a fractional frequency reuse (FFR) technique to manage the interference in the proposed variable-height UAV based network. To the best of our knowledge, this is the first paper where circle packing and FFR have been exploited to manage interference where omnidirectional antennas are used, contrasting with [5], [7], [20] which only focused on equal-size circle packing models using directional antennas and with [17], where omnidirectional antennas are used without modelling the interference. To this end, we optimize the FFR cell partitions to maximize the area spectral efficiency (ASE) of the network and compare the optimal results of the models for a given set of UAVs.

This paper is organized as follows. We introduce the multi-tier UAV deployment configuration, describe the AtG channel model and cell association policy in section II. The two-tier UAV deployment design is elaborated in section III. The RL based UAV height optimization method is detailed in section IV. The aerial base station (ABS) transmit power control and FFR based resource allocation policies and cell partition optimization are presented in section V. The performance evaluation metrics and relevant results are presented and discussed in section VI. In section VII, an extension to higher tiers is proposed and relevant results are presented. We conclude the paper in section VIII.

II. PROPOSED SYSTEM MODEL

A. MULTI-TIER VARIABLE HEIGHT UAV DEPLOYMENT

Given the agility and mobility of UAVs, a major question is how to deploy and adaptively manage a set of UAVs to best cater for wireless traffic in a specific region under an emergency or on-demand scenario. Therefore, we investigate the problem of coverage maximization and resource allocation for a number of ABSs M providing wireless coverage within a coverage region of radius R. Considering the employment of either omnidirectional or directional antennas at ABSs and we address this problem by investigating three distinct sub-problems:

1) **User coverage maximization** within the overall coverage region is studied by determining the coverage areas of individual ABSs (i.e., position and area of individual cells).
2) **UAV height optimization** is investigated for each ABS to provide highest QoS for users within their determined cell areas.
3) An **FFR scheme** is developed to effectively manage interference among neighboring cells and to enhance average spectral efficiency (SE).

It is well known that the complexity of optimal UAV placement increases with the number of UAVs. Furthermore, research shows that for realistic path loss (PL) exponents the cell shape is near-circular for directional and omnidirectional antennas [32]. Hence, the first problem above can be formulated as a circle packing problem. To address this, authors of [5] considered the equal-size circle packing for multi-UAV deployments using directional antennas. However, this model inherently suffers from random uncovered areas as shown in Figure 1(a).

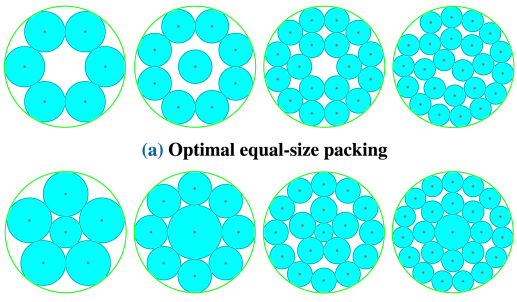

(a) Optimal equal-size packing

(b) Variable-size packing

FIGURE 1. An illustration of the optimal equal-size circle packing and the proposed UAV deployment using variable-size circle packing: Four random use cases for comparison.

To fully exploit the flexibility of UAV-based ABSs for 3D deployment and noting that variable heights of ABSs map into the variable size of their circular footprints, we investigate variable-size circle packing problem in contrast to [5]. In order to complete the 3D (x, y, z) deployment, the horizontal coordinates (x, y) are represented by the center of the circles, while the z-coordinate is defined by the height of an ABS. However, assuming no constraint other than maximizing the coverage area of the UAV network, the variable-size circle packing problem may lead to extreme, impractical or non-converging solutions, e.g., a very large ABS footprint in the center while remaining footprints becoming very small. Here, we propose a multi-tier variable height UAV deployment solution, Figure 1(b) depicts a top-down view of the proposed scheme, where the size of the circles are constant in each tier but they can change across tiers. The proposed approach includes a single central UAV allocated to tier 1 and the rest of UAVs being located around it in one or possibly more additional tiers, while the neighboring circles in each tier are tangential to each other. The proposed multi-tier ABS deployments provide a systematic approach for the cellular design while improving the coverage compared to the equal-size circle packing solution by exploiting the ability of UAV-based ABSs to be deployed at different

heights, completing the cellular design of the UAV-based network. We then optimize UAV heights according to the variable size of the cells and devise an effective resource allocation scheme.

B. CHANNEL MODEL

We consider a realistic AtG channel model in this work where PL on both LoS and non-LoS (NLoS) components of the communication link is considered. The LoS probability is defined as [33]

$$P_{\text{LoS}}^{mk} = \frac{1}{1+\alpha_1 \exp\left(-\alpha_2\left[\frac{180}{\pi}\arctan\left(\frac{h_m}{r_{mk}}\right)-\alpha_1\right]\right)}, \tag{1}$$

where α_1 and α_2 are constant parameters which depend on carrier frequency and the communication environment, h_m is the height of the mth ABS and r_{mk} is the kth user's ground distance from the projection of the mth ABS. Also, the probability of the NLoS link $P_{\text{NLoS}}^{mk} = (1-P_{\text{LoS}}^{mk})$. The PL for both links can be independently defined as [12]

$$PL_{mk} = \begin{cases} \gamma_1\left(\frac{4\pi f_c\sqrt{r_{mk}^2+h_m^2}}{c}\right)^{\eta}, & \text{LoS link,} \\ \gamma_2\left(\frac{4\pi f_c\sqrt{r_{mk}^2+h_m^2}}{c}\right)^{\eta}, & \text{NLoS link,} \end{cases} \tag{2}$$

where γ_1 and γ_2 ($\gamma_2 > \gamma_1 > 1$) are the excessive PL coefficients for the respective LoS and NLoS scenarios, f_c is the carrier frequency, η is the PL exponent and c denotes the speed of light. Now, the average PL in the downlink that considers both LoS and NLoS components can be stated as

$$PL_{mk}^{av} = P_{\text{LoS}}^{mk}\gamma_1\left(\frac{4\pi f_c\sqrt{r_{mk}^2+h_m^2}}{c}\right)^{\eta} + P_{\text{NLoS}}^{mk}\gamma_2\left(\frac{4\pi f_c\sqrt{r_{mk}^2+h_m^2}}{c}\right)^{\eta}. \tag{3}$$

Note that the average PL in (3) captures the effect of shadowing by incurring additional loss in the AtG link. We ignore the impact of small-scale fading which is largely ignored by several key studies on UAV networks including [7], [34], [35]. As the circle packing based state-of-the-art UAV deployments revolve around directional antennas as a benchmark application, we first present the case when directional antennas are employed. The position of each ABS in any tier is a function of the antenna beamwidth θ_w, the coverage radius r_m, and the height h_m, $\forall m \leq M$. Using the ABS antenna's half-power beamwidth θ_w, we approximate the antenna gain as [36]

$$G_D = \begin{cases} \frac{G_0}{{\theta_w}^2}, & \frac{-\theta_w}{2} \leq \phi \leq \frac{\theta_w}{2}, \\ g(\phi), & \text{otherwise,} \end{cases} \tag{4}$$

where $\frac{G_0}{{\theta_w}^2}$ is the directional antenna main lobe gain with $G_0 \approx 29000$. Also, in practice $0 < g(\phi) \ll G_0/{\theta_w}^2$, we therefore assume, the antenna power gain $g(\phi)$ to be insignificant outside the main-lobe, and it is ignored. Then the received power for the kth user associated with ABS m is given as

$$\zeta_{r,d}^{mk} = \frac{\zeta_t^m 10^{\frac{G_0}{10\theta_w^2}}}{\left(L_0(Q_0\sqrt{r_{mk}^2+h_m^2})^{\eta}\right)}, \tag{5}$$

where $L_0 = P_{LoS}^{mk}\gamma_1 + P_{NLoS}^{mk}\gamma_2$, $Q_0 = \frac{4\pi f_c}{c}$, ζ_t^m is the transmit power of ABS m and the subscript d indicates the directional antennas case.

For the omnidirectional antenna case, which is the main focus of this work, the average PL is inverted [33], [37] to obtain the average channel gain. Then, received power for the kth user associated with ABS m can be expressed as

$$\zeta_{r,o}^{mk} = \frac{\zeta_t^m}{\left(L_0(Q_0\sqrt{r_{mk}^2+h_m^2})^{\eta}\right)}, \tag{6}$$

where subscript o represents the case involving omnidirectional antennas.

C. USER DISTRIBUTION AND CELL ASSOCIATION

We consider K users are uniformly and independently distributed inside the coverage area using homogeneous Poisson point process which is obtained through a spatial point process. The kth user's random location is denoted by (x_k, y_k). For the directional antenna case, considering that the mth ABS is located at (x_m, y_m), then the user is associated with ABS m when $r_{mk} \leq r_m$, where $r_{mk} = \sqrt{(x_k-x_m)^2+(y_k-y_m)^2}$ is the ABS to user ground distance and $r_m = h_m \tan(\theta_w/2)$. In case of omnidirectional antennas, we consider a widely used cell association policy known as reference signal received power (RSRP) due to the flexibility it offers to the users. Since we adjust the transmit power of each ABS relative to its cell size, unlike directional antenna case the users located outside the ABS footprints cannot be ignored. Therefore, the policy allows users to be associated with an ABS that provides the strongest RSRP as

$$m^* = \arg\max_{m \in M}, \quad RSRP_{mk}. \tag{7}$$

Let s_k denote the selection of user k, we indicate whether k is associated with ABS m using an indicator $\mathcal{I}_{mk}$ as follows

$$\mathcal{I}_{mk} = \begin{cases} 1, & s_k = m \\ 0, & s_k \neq m. \end{cases} \tag{8}$$

Moreover, to facilitate the resource allocation we assign users to a cell association vector Γ_m (when $\mathcal{I}_{mk} = 1$) to denote the number of users and their location (x_k, y_k) information for each ABS.

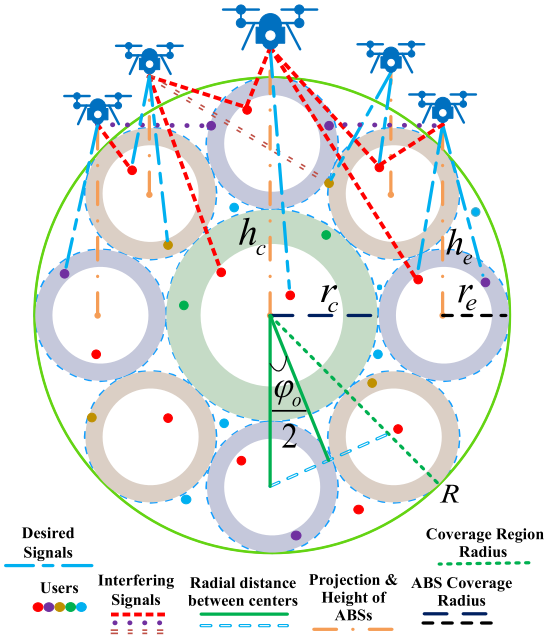

FIGURE 2. Cell configuration for the proposed two-tier variable height UAV network.

III. TWO-TIER VARIABLE HEIGHT UAV-BASED CELLULAR NETWORK

The two-tier UAV deployment is first introduced here before being extended to multiple tiers of more than two in section VII. In this model, we assume all ABS footprints are tangential with neighboring cells to maximize the coverage while limiting the inter-cell interference (ICI) based on the non-overlapping design. This principle ensures a unique two-tier solution for the UAV network when the number of ABSs $M \geq 4$ based on which the location of ABSs can be exactly determined. Note that this unique solution coincides with the optimal equal-size circle packing solutions for $M = 7$ but it gives a variable height two-tier deployment in general.

Considering the coverage radii of ABSs in tier-1 and tier-2 in Figure 2 to be r_c and r_e, respectively, we can express their relationship with the coverage region radius R as $R = r_c + 2r_e$. Using the central angle property for a chord that is created between two tangent footprints of ABSs in tier-2, we have

$$r_e = \frac{r_c \sin(\varphi_o/2)}{1 - \sin(\varphi_o/2)}, \tag{9}$$

$$R = r_c + \frac{2r_c \sin(\varphi_o/2)}{1 - \sin(\varphi_o/2)}, \tag{10}$$

where $\varphi_o = 2\pi/M_2$ is the central angle from the origin of the coverage region and M_2 is the number of circles in the second tier, which is $M_2 = M - 1$ for the two-tier network. Solving for r_c we get

$$r_c = \frac{1 - \sin(\varphi_o/2)}{1 + \sin(\varphi_o/2)} R, \tag{11}$$

similarly,

$$r_e = \frac{\sin(\varphi_o/2)}{1 + \sin(\varphi_o/2)} R. \tag{12}$$

The coverage density is defined as the area covered divided by the total area. We can calculate the coverage density D_V for any number of available ABSs under two-tier network model as

$$D_V = \frac{r_c^2 + (M-1)r_e^2}{R^2} = \frac{1 + M\sin^2(\varphi_o/2) - 2\sin(\varphi_o/2)}{(1 + \sin(\varphi_o/2))^2}. \tag{13}$$

The coverage density D_E for the equal-size circle packing can be also calculated as a benchmark as [5], [38]

$$D_E = \frac{M\mu_n^2}{(2 + \mu_n)^2}, \tag{14}$$

where the optimal value of the variable μ_n can be obtained by solving

$$\frac{\pi(\sqrt{4 - \mu_n^2} + \mu_n\sqrt{3})}{\mu_n \arcsin(\mu_n/2)} + 2\sqrt{3}(1 - M) = 0, \tag{15}$$

and the corresponding optimal radius of the equal-size circles is given by

$$r_0 = \frac{\mu_n}{(2 + \mu_n)} R. \tag{16}$$

We employ quasi-stationary ABSs in this work; that is, the position of these ABSs is not changed unless a redeployment is initiated. It is crucial to find the horizontal coordinates of the ABSs to ensure rapid deployment and also to avoid collisions. For the two-tier network, the first UAV is placed at the horizontal coordinates $H_1 = [0, 0]$ (i.e., the center of the coverage area) as the tier-1 ABS and the rest of UAVs comprise the tier-2 ABSs. The horizontal coordinates of tier-2 UAVs (i.e., $H_m, \forall\, 2 \leq m \leq M$) can be calculated using (11) and (12) as

$$H_m = R_p\big[\cos(\theta_r + \varphi_o(m-2)), \sin(\theta_r + \varphi_o(m-2))\big], \tag{17}$$

where $R_p = r_c + r_e$, and θ_r can be randomly chosen in the range $[0, 2\pi]$. Without loss of generality, we use $\theta_r = \pi/2$ unless stated otherwise. Algorithm 1 summarizes the method for the calculation of the position and radii of individual ABS footprints for the proposed two-tier UAV cellular network design.

Note that the coverage radii of a set of M ABSs can be readily determined using (11) and (12) as a function of the radius of coverage region for a two-tier network. One can observe that the coverage footprint of the central ABS increases with M. Therefore, we consider the UAV allocated for the central ABS to be more resourceful in terms of mechanical design and transmit power capability. This assumption is practical as this ABS can play an additional role of coordination with the command and control center. Nevertheless, practical constraints (e.g., maximum transmit

Algorithm 1 Proposed Two-Tier UAV Cellular Design

Input : Coverage area radius, R
Number of ABSs, M
Output: Horizontal locations of ABSs, $H_m(\forall\, 1 \leq m \leq M)$
cell radius for tiers 1 and 2, (r_c, r_e)
initialize;
$\theta_r = \pi/2$
Calculate angles $\varphi_o = 2\pi/(M-1)$
Find r_e from (12), r_c from (11) using φ_o, and R
Set $H_1 = [0, 0]$
Find H_m from (17)
return r_c, r_e, $H_m(\forall\, 1 \leq m \leq M)$.

power, height, UAV's mechanical design, etc.) may prevent a substantial increase of the central ABS coverage footprint. Therefore, in order to sustain a good overall user coverage and throughput performance, we need to transition from the two-tier network to a three-tier network (and eventually to n tiers) when M increases beyond a certain value as will be discussed later in section VII.

IV. ABS HEIGHT OPTIMIZATION USING REINFORCEMENT LEARNING

In comparison to terrestrial links, the AtG links have inherent advantages of lower PL exponents and reduced fading effects but the longer link lengths can deteriorate the SNR. These two contrasting effects can be balanced by adjusting the heights of the ABSs. Our objective for the height optimization is to maximize the average user QoS within each cell measured by the average cell throughput, which can be expressed as users' achievable SE measured in bits/s/Hz. The SE for the kth user covered by the mth ABS cell is given as

$$SE_k^m = \log_2\left(1 + \frac{\zeta_t^m / PL_{mk}}{I_T^k + N_p}\right), \tag{18}$$

where I_T^k and N_p are the total interference caused by adjacent ABSs and noise power, respectively. Note that the ABS's height and the interference it generates towards the other cells are tightly coupled and this adds complexity to the height optimization in a multi-UAV network [39]. Hence, the use of SINR metric for rate calculations when simultaneously optimizing the height of M ABSs is extremely challenging, if not impossible. Consequently, following [16] we choose the SNR metric and neglect the interference term in (18). This assumption can be justified based on the FFR technique proposed in the next section to substantially reduce the inter-cell interference within the network.

Since coverage areas of the ABSs are predefined and users are assumed to be uniformly distributed, the average number of users in each cell is proportional to its size. Hence, we formulate the problem to be independent of the number of users and their individual locations by focusing on the average user performance. As depicted in Figure 3, we make the problem

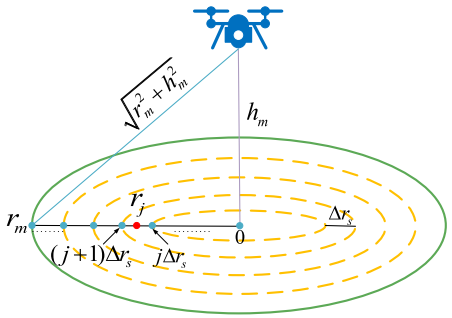

FIGURE 3. An illustration of an ABS cell divided into circular rings with radius of jth ring r_j and ring width Δr_s.

consistent with the cell size by dividing each cell into several rings where the radius and width of the jth ring are denoted by r_j and Δr_s, respectively. There are $l = r_m/\Delta r_s$ total rings. Noting the radius of jth ring as $r_j = \Delta r_s(2j+1)/2$, the area of the jth ring in the mth ABS cell can be approximated as

$$\mathcal{A}_{j,m} = 2\pi r_j \Delta r_s, \tag{19}$$

and the average number of users in the jth ring can be denoted by

$$K_{j,m} = \frac{\mathcal{A}_{j,m}}{\pi r_m^2}\overline{K}_m = \frac{2r_j\Delta r_s}{r_m^2}\overline{K}_m, \tag{20}$$

where $\overline{K}_m$ is the total number of users located inside the coverage footprint (i.e., $r_{mk} \leq r_m$). Assuming all the rings are assigned bandwidth proportional to their size (i.e., equal bandwidth allocation among the users). Then, the bandwidth assigned to the jth ring is given by

$$W_{j,m} = \frac{K_{j,m}}{\overline{K}_m} W_m, \tag{21}$$

where W_m is the bandwidth assigned to each cell. The average throughput of the jth ring can be stated as

$$\mathcal{R}_m(r_j) = W_{j,m} SE_m(r_j). \tag{22}$$

Assuming that l is sufficiently large, the average cell throughput of the mth ABS cell can be well approximated by calculating the following summation

$$\mathcal{R}_m^{ABS} = \sum_{j=1}^{l} \mathcal{R}_m(r_j). \tag{23}$$

Finally, the optimal height h_m^{opt} can be obtained by solving the following optimization problem (OP) for each cell

$$h_m^{opt} = \arg \max_{h_{\min} \leq h_m \leq h_{\max}} \mathcal{R}_m^{ABS}. \tag{24}$$

The OP in (24) is not analytically tractable due to the nonlinear objective function which depends on the average PL of users at different locations. The lower bound of the feasible set for this OP, $h_{\min}$ is defined as 10m [40]. Note that, as height of ABS increases the received signal level at all locations away from the cell center increases initially but

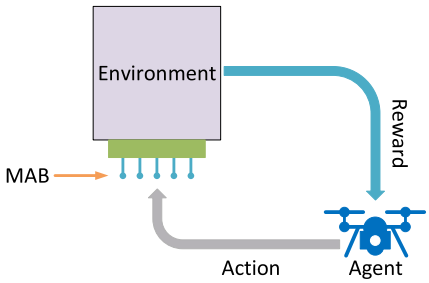

FIGURE 4. The concept of multi-armed bandit (MAB) learning.

then decreases beyond a threshold. For a cell edge user, such threshold denoted by h_m^{edge} would be highest among all users within the cell. Hence, we use h_m^{edge} as the upper bound on the height ($h_{max} = h_m^{edge}$) for each cell as beyond this height the PL for all users increases. In order to find h_m^{edge}, we first convert (3) into the logarithmic form as

$$PL_{mk}^{av}(dB) = \frac{\gamma_1 - \gamma_2}{1 + \alpha_1 \exp\left(-\alpha_2\left[\theta_{edge} - \alpha_1\right]\right)} + 20\log\left(\frac{4\pi f_c\sqrt{r_m^2 + h_m^2}}{c}\right) + \gamma_2,$$

where $\theta_{edge} = \frac{180}{\pi}\arctan(\frac{h_m}{r_m})$ is the elevation angle of an edge user. Note that h_m^{edge} is the optimal height that minimizes the PL of the edge user. Hence, by taking the partial derivative $\frac{\partial r_m}{\partial h_m} = 0$ we obtain [12]

$$\frac{\pi h_m}{9\ln(10)} + \frac{r_m\alpha_1\alpha_2\gamma_d \exp\left(-\alpha_2\left[\theta_{edge} - \alpha_1\right]\right)}{\left(\alpha_1 \exp\left(-\alpha_2\left[\theta_{edge} - \alpha_1\right]\right) + 1\right)^2} = 0, \quad (25)$$

where $\gamma_d = (\gamma_1 - \gamma_2)$. At an optimal elevation angle, the coverage radius is maximized for a predefined PL value. Equivalently, there is an optimal height at which the PL at cell edge is minimized for a given coverage radius. Therefore, we solve (25) to obtain h_m^{edge}, which is widely used for determination of optimal height in UAV networks [12], [16], [17], [31].

Here, we consider a computationally efficient RL algorithm (see Algorithm 2) to determine the solution to the OP in (24) for each ABS cell. In RL, an agent discovers the best action (i.e., height) which yields the most reward (i.e., average cell throughput) through a process of trial and error. With the uniform user distribution and ring-based approximation elaborated in Figure 3, this scenario perfectly aligns with a markov decision process (MDP) with a single state (i.e., stationary environment) which can be optimally handled with RL-based multi-armed bandit (MAB) problem [41]. The aim of MAB is to develop a learning policy that achieves maximal cumulative reward. The concept of RL-based MAB is depicted in Figure 4.

In RL-MAB problems, action selection method is of crucial importance. One fundamental RL action selection approach is known as greedy action policy which selects an action $\mathcal{H}$ at time t with the highest estimated reward using

$$\mathcal{H}_t = \arg\max_h Q_t(h), \quad (26)$$

where $Q_t(h)$ is the mean reward when a particular action (height h) is selected. However, the greedy policy might be short-sighted as it tries to maximize the immediate reward by exploiting the environment; spending no time to explore it for the long-term future rewards. An efficient alternative is the ϵ–greedy policy, where ϵ refers to the probability of opting to explore the environment while agent exploits with the probability $1 - \epsilon$. This RL technique is computationally efficient because it incrementally updates the average reward which requires an insignificant memory and computation resource. That is, record of all the previous rewards is not required. Denote Q_n and R_n as the estimated and nth reward, respectively, the updated average of all n rewards is then computed as [42]

$$Q_{n+1} = Q_n + \frac{1}{n}\left[R_n - Q_n\right], \quad (27)$$

where $Q_n = \sum_{i=1}^{n-1} R_i$ represents an estimated reward value when a particular action is selected $n - 1$ times.

Algorithm 2 ABS Height Optimization Using RL

Input : Height lower h_{min} and upper h_m^{edge} bounds, coverage radius r_m, iterations $\mathcal{N}$
Output: Optimal ABS height h_m^{opt}
initialize;
Height action values h_{min} to h_m^{edge} with step size δ_h
$Q(h) \leftarrow 0$
$N(h) \leftarrow 0$
for $ItNnum = 0 : \mathcal{N}$ **do**
  $\mathcal{H} \leftarrow \begin{cases} \arg\max_h Q(h), & \text{prob. } 1-\epsilon, \\ \text{select a random action}, & \text{prob. } \epsilon, \end{cases}$
  Compute reward R_w for action $\mathcal{H}$ using (23)
  Increment the action count:
  $\mathrm{N}(\mathcal{H}) \leftarrow \mathrm{N}(\mathcal{H}) + 1$
  Update the mean reward:
  $Q(\mathcal{H}) \leftarrow Q(\mathcal{H}) + \frac{1}{N(\mathcal{H})}\left[R_w - Q(\mathcal{H})\right]$
end
return $\mathcal{H}$ as h_m^{opt} with highest reward $Q(\mathcal{H})$

The number of iterations $\mathcal{N}$ in RL-MAB based algorithms is predefined and it is unaffected by the state space. Consequently, one can see that the complexity of Algorithm 2 is $\mathcal{O}(\mathcal{N})$. To ensure a fast convergence under this RL technique, it is important to properly calibrate the value of ϵ. Figure 5 shows the convergence comparison of the employed ϵ-greedy method with different values of ϵ along with the optimistic and ϵ-decay policies as benchmarks. For the optimistic policy, an optimistic value of the reward is obtained using a height value of 200m [43] and the average cell throughput

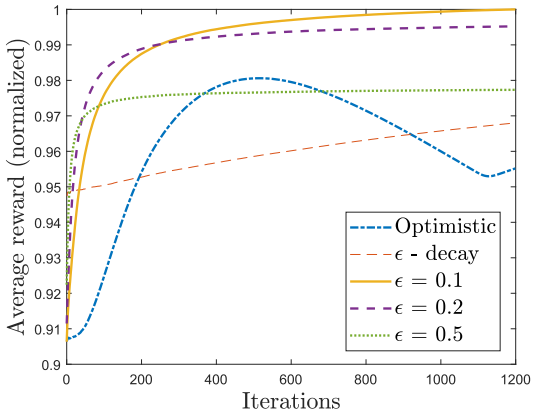

FIGURE 5. A performance comparison under three ϵ-greedy values, ϵ-decay, and optimistic approach after 1200 iterations for an ABS cell of coverage radius = 300*m*.

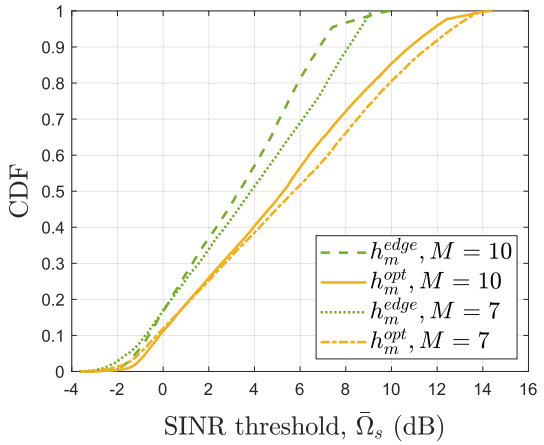

FIGURE 6. CDF of SINR for two use cases of ABSs ($M = 7, 10$) using the proposed h_m^{opt} and commonly used h_m^{edge} ABS height optimization methods.

is computed using (23). Under the ϵ-decay policy, the probability of exploration is reduced with every iteration i using $\epsilon(i) = \frac{1}{1+i\varrho}$, $\varrho < 1$ is the scaling factor. These results indicate that the ϵ-greedy algorithm outperforms other two closely related policies, ϵ-decay and the optimistic policy. Based on these trials, $\epsilon = 0.1$ is selected for the proposed height optimization as the algorithm performs better compared to the other values (i.e., $\epsilon = 0.2, 0.5$) used during the trial. Similarly, for the directional antenna case, we can optimize the height using the same OP in (24). In this case, the values of h_{min} and h_{max} can be calculated in terms of the directional antenna beamwidth limits θ_{min} and θ_{max} based on the following relationship

$$h_m = r_m \cot(\theta_m/2), \quad \forall m \in M. \tag{28}$$

We now demonstrate the results in Figure 6 which exhibits the CDF of SINR for two deployment use cases ($M = 7, 10$) with two different height optimization methods, Algorithm 2 (h_m^{opt}) and widely used cell-edge PL minimization (h_m^{edge}) determined by solving (25). We obtained these results by adjusting the transmit power of ABSs (detailed in next section) to achieve a minimum received power at cell edges when the optimal heights h_m^{opt} $\forall m \in M$ are considered, while the same transmit powers are allocated to the ABSs in the h_m^{edge} method for a fair comparison. Clearly, these results show that for any given SINR threshold more users are in outage under the h_m^{edge} approach compared to our proposed height optimization approach. It is evident that the proposed h_m^{opt} method outperforms its counterpart in both equal and unequal ABS cell size cases using the same system parameters. Essentially, it is because under the h_m^{edge} method, ABSs fly relatively higher as depicted by the 3D deployments in Figure 7(a) and Figure 7(b). Since h_m^{edge} method only concerns with the boundary user, it also increases the interference affecting other cells (due to a higher elevation angles). Moreover, in UAV-assisted networks LoS connection for the users closer to cell center is very reliable but as the ABSs fly further high, PL in h_m^{edge} method increases due to an increased distance between ABS and user, which in turn decreases average SINR levels. Intuitively, the ABSs also consume more energy for propulsion to reach the higher altitudes under the h_m^{edge} method while a higher transmit power (on the average) will be required from the users if the uplink transmissions are considered. Hence, the UAV height optimization based on edge user is not energy-efficient, not just in terms of average received powers in the downlink and uplink, but also from the mechanical energy consumption viewpoint. By contrast, our approach is more energy-efficient and reliable.

V. RESOURCE ALLOCATION POLICIES

A. EDGE ADAPTIVE TRANSMIT POWER CONTROL

It is commonly assumed in the FFR networks that the downlink transmit power is equal for both center and edge regions [44]. Therefore, once the height of ABSs is optimized, the transmit power of ABSs can be adjusted to guarantee a minimum received power $\zeta_{r,edge}^{min}$ at the cell-edge, which not only ensures a minimum QoS to all the users inside the cells (in the absence of interference) but also dictates the coverage of each ABS cell corresponding to its size. Therefore, we adjust this power using

$$\zeta_t^m = \zeta_{r,edge}^{min} PL_{edge}^m, \tag{29}$$

where PL_{edge}^m is the PL at the cell-edge of ABS m.

To ensure a fair comparison between the proposed variable height cellular design with variable allocated power and the benchmark equal-height cellular design with constant power, the transmit power of all ABSs in the proposed scheme are averaged to determine the constant transmit power of each ABS in the equal-height UAV network.

Note that the irregular geometries in the equal-height UAV network and the variable heights of UAVs in the variable-height UAV network would lead to varying interference levels particularly at the cell edges. To illustrate this, we plot 3D coverage patterns along with the ABS projection coordinates

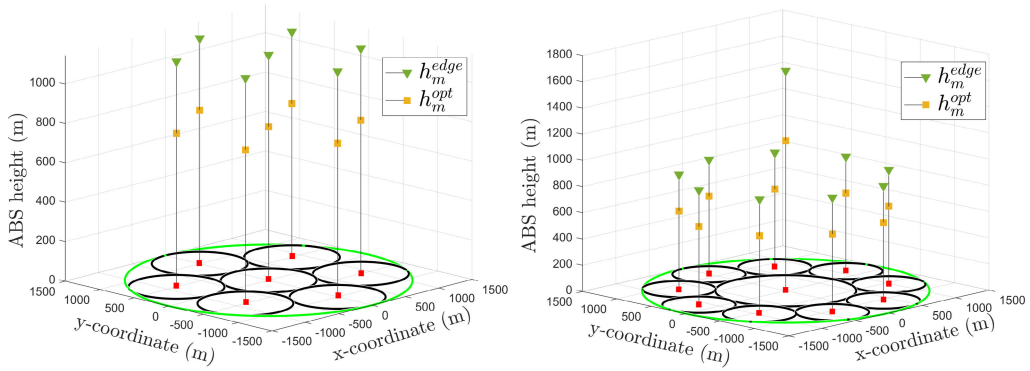

(a) 7 ABSs (b) 10 ABSs

FIGURE 7. 3D deployment of ABSs using two height optimization methods h_m^{opt} and h_m^{edge} for two use cases.

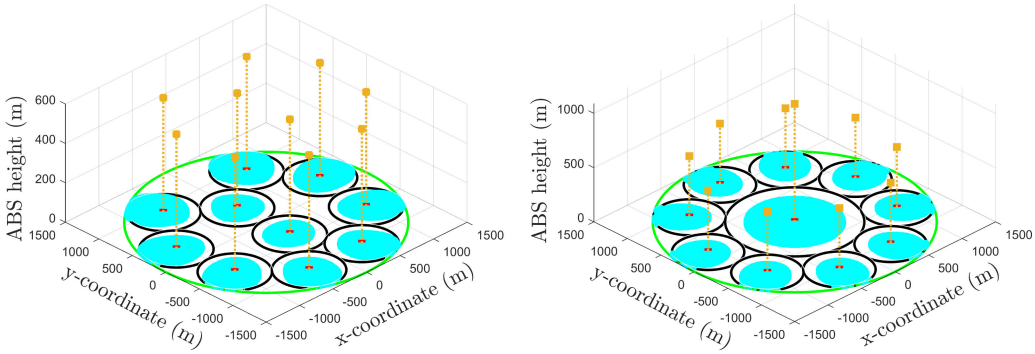

(a) $\mathcal{M}_E$, 10 ABSs (b) $\mathcal{M}_V^2$, 10 ABSs

FIGURE 8. Coverage map with 3D deployment of ABSs for the two models under the use case $M = 10$, the cian patches represent users satisfying the SINR threshold ($\bar{\Omega}_s$= 6 dB) without FFR.

in Figure 8 when FFR is not considered. An SINR threshold of $\bar{\Omega}_s = 6$ dB is used to obtain these coverage maps after 2×10^3 Monte Carlo trials. The cian patches depict coverage region of ABSs where users are satisfying the threshold requirement when FFR is not considered. It can be noticed that the edge users suffer more due to severe interference generated by the neighboring ABSs. This impact is more adverse on the edge users of relatively small ABS cells as strong interference is directed from the central ABS. However, the central ABS' coverage is also considerably affected due to the presence of $(M - 1)$ neighboring interferers. Interestingly, edge users in the equal-height UAV deployments also encounter severe interference in several cells due to an irregular placement of cells. To cope with this strong ICI, we apply FFR to enable a tradeoff between high SE and good overall user experience.

In this work, we use a more practical *static* FFR technique [45] in which all the system parameters are configured in advance and are not subject to change for a certain period of time. Frequency partitioning in FFR is attained by allocating a set of frequencies to the center users that are reused in all the cells under a frequency reuse of Δ_C (FR-Δ_C) while distinct subbands are exercised across the cell edges with a frequency reuse of Δ_E (FR-Δ_E), where $\Delta_E > \Delta_C$. In order to evaluate the performance of the network under uniform resource allocations, we adopt a widely used resource allocation strategy ($\Delta_C = 1$, $\Delta_E = 3$) as shown in Figure 9.

Unlike the variable-height UAV network, the footprint placements (circles) in equal-height network are quite random i.e., coverage pattern changes significantly for different number of ABSs. We adopt the method employed in [46] for the cell-edge frequency selection based on the reuse distance. Also, when an odd number of ABSs cover tier-2 of the proposed network, we encounter a resource allocation problem using $\Delta_E = 3$. This is because we alternatively use two sets of frequencies ($\mathcal{F}_3$, $\mathcal{F}_4$) in tier-2 but with odd number of ABS cells in tier-2 (odd M_2) two adjacent ABSs end up using the same frequency set. However, this problem can be easily tackled by equipping at least one ABS cell with a sectorized omnidirectional antenna [47], which is active to send or receive signals primarily through an angular sector employing two different frequency sets $\mathcal{F}_3$ and $\mathcal{F}_4$ (different than the adjacent ABS on each side) having an angle of no more than 180°.

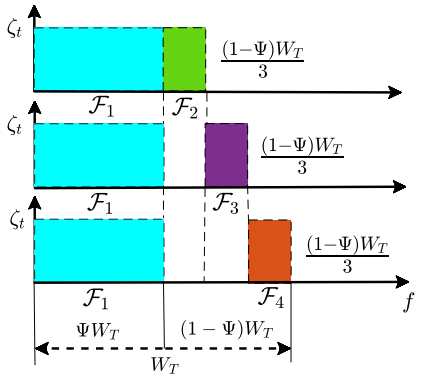

FIGURE 9. Resource allocation in FFR system with $\Delta_E = 3$.

B. BANDWIDTH ALLOCATION

We analyze the performance of our network models under frequency division multiple access (FDMA)-based FR-Δ_C and FR-Δ_E schemes for the center and edge regions, respectively. We consider the FDMA-based scheme as they can be efficiently mapped into corresponding orthogonal-FDMA-based allocations involving frequency band partitioning into multiple physical resource blocks [48].

The SINR of kth user under the FFR scheme can be expressed as

$$\begin{aligned} \text{SINR}_{\text{mk}} &= \frac{\zeta_t^m / PL_{mk}}{I_T^k + N_p}, \\ \text{SINR}_{\text{mk}} &= \frac{\zeta_t^m / PL_{mk}}{\sum_{n \in \mathcal{J}_k} \zeta_t^n / PL_{nk} + N_p}, \end{aligned} \tag{30}$$

where noise power N_p depends on the noise spectral density N_0 and user equipment noise figure δ_{UE}. Also, $I_T^k = \sum_{n \in \mathcal{J}_k} \zeta_t^n / PL_{nk}$, $n \neq m$, is the ICI power which depends on the interfering cell set $\mathcal{J}_k$ of user k. The interfering set depends on the user location and cell association. For example, $\mathcal{J}_k = \mathcal{J}_C$ when the user is located in the center region as shown with the subband set $\mathcal{F}_1$ in Figure 9. While $\mathcal{J}_k = \mathcal{J}_E$ for a set containing cells using one of the three subbands (e.g., $\mathcal{F}_2$) for the edge region. Moreover, as the center and edge regions are partitioned, interference directed towards the edge users is substantially reduced. However, each cell is now allocated $\Delta_C + 1$ of the total $\Delta_C + \Delta_E$ subbands. Note that the subband partitioning impacts the overall resource efficiency (i.e., ASE) but in contrast, improves the average SINRs of the users.

The FFR scheduler allocates the total bandwidth, $W_T = W_C + W_E$. In order to effectively manage the bandwidth partition, we define Ψ as the normalized FR bandwidth $\Psi = \frac{W_C}{W_T}$, $0 \leq \Psi \leq 1$. Furthermore, W_E is divided among the edge users depending on the Δ_E employed. Therefore, the total available bandwidth to each cell is

$$\begin{aligned} W_m &= \Psi W_T + \frac{1}{\Delta_E}(1-\Psi)W_T, \\ &= W_{\Delta_C} + W_{\Delta_E}. \end{aligned} \tag{31}$$

C. CELL PARTITION OPTIMIZATION

Typical threshold based center and edge users classification methods (i.e., fixed distance, received power, fixed SINR) are effective where cells are characterized by almost equal performance levels, which is not the case here. To consider the variable nature of the proposed cellular design, we adopt a user classification method, where the SINR threshold is optimized for each cell by maximizing its SE. In this approach, first users associated with each cell measure received pilots or data symbols to acquire received SINRs. Then, users with SINRs above the threshold $\bar{\Omega}_{th}$ are classified as center users, otherwise as edge users. Once the spectrum allocation is decided, performance of the network in terms of throughput and SE is ultimately determined by the SINR thresholds. The SE level realized at the kth user is denoted by $\Phi_{\upsilon,k} = \frac{1}{\Delta_\upsilon} \log_2\left(1 + \Omega_{\upsilon,k}\right)$ [49], where $\upsilon = C, E$ and $\Omega_{\upsilon,k}$ denotes the SINR of the kth user. The SINR threshold OP can be split into M sub-problems, for each cell as follows

$$\hat{\Omega}_{th}^m = \arg \max_{0 \leq \bar{\Omega}_{th} < \infty} \sum_{\forall k} \Phi_{C,k} + \sum_{\forall k} \Phi_{E,k}. \tag{32}$$

This is a nonlinear OP and it depends on the SINR of multiple users at random locations, which makes the problem extremely hard to solve. Assuming the channel-state information is known at the ABS, we can use a similar RL-based approach as Algorithm 2 to find optimal SINR threshold to solve the OP in (32). To avoid redundancy, we omit the pseudo-code here which is similar to the Algorithm 2, the following parameter settings are employed. We select and input a large action window of SINR threshold $\bar{\Omega}_{th}(\text{dB}) \in [-10, 15]$ to rigorously find an optimal SINR threshold that maximizes the SE of the cell. A number of actions is initialized using an action step size $\delta_s = 0.05$. For each selected action of the SINR threshold the cell is partitioned into center and edge regions and the objective function in (32) is evaluated to converge to an optimal $\hat{\Omega}_{th}^m$ that maximizes the SE of the mth cell. The ϵ-greedy algorithm is run individually for all the M sub-problems to achieve an overall network SE maximization.

VI. COVERAGE AND THROUGHPUT ANALYSIS OF FFR-AIDED UAV NETWORK

In this section we present three widely used performance metrics namely coverage probability, rate coverage, and ASE followed by corresponding simulation results to evaluate and compare the performance of our proposed ABS deployment techniques.

A. NETWORK PERFORMANCE METRICS

The coverage probability is one of the most significant metrics to evaluate the reliability of the probabilistic AtG channel. It can be defined as

$$\mathcal{P}_c = \mathbb{P}[SINR \geq \bar{\Omega}_s], \tag{33}$$

where $\mathbb{P}[.]$ is the probability operator and $\bar{\Omega}_s$ is the minimum SINR required by the user in order to be covered.

TABLE 1. Simulation parameters.

Parameters	Values
System bandwidth, W_T	30 MHz
Carrier frequency, f_c	2 GHz
Coverage radius, R	1500 m
Number of users, K	600
Noise power density, N_0	-170 dBm/Hz
User equipment noise figure, δ_{UE}	9 dB
Additional path loss LoS, NLoS, (γ_1, γ_2)	3 dB, 23 dB
Environment parameter, (α_1, α_2)	12.08, 0.11
Minimum edge power, $\zeta_{r,edge}^{min}$	-80 dBm
Directional antenna beamwidth, (θ_{min}, θ_{max})	50°, 120°

The coverage probability of the kth user associated with mth ABS considering an aggregate interference I_T^k can be defined as

$$\mathcal{P}_c = \mathbb{P}\left[\frac{\zeta_r^{mk}}{I_T^k + N_p} \geq \bar{\Omega}_s\right] = \mathbb{P}\left[\zeta_r^{mk}(dB) \geq \zeta_{r_{min}}\right], \quad (34)$$

where ζ_r^{mk} is the received power in the interference-free scenario. Also, $\zeta_{r_{min}} = 10\log_{10}(\bar{\Omega}_s I_T^k + \bar{\Omega}_s N_p)$ is the minimum required received power for the kth user in the presence of interference and I_T^k depends on the interfering set $\mathcal{J}_k$. Rate coverage probability is an important metric which is used to evaluate the network performance in terms of user achievable data rates. This metric extends the performance evaluation beyond SINR coverage because it entails the resource allocation and user load on the network. In order to be covered, the data rate $\mathcal{R}_k$ of an arbitrary kth user must meet or exceed the target rate threshold $\bar{\mathcal{R}}_{th}$ (bits/s). Then, the rate coverage can be defined as

$$\mathsf{R}_c = \mathbb{P}[\mathcal{R}_k \geq \bar{\mathcal{R}}_{th}]. \quad (35)$$

We consider the bandwidth available to the center and edge regions is equally divided among the users to perform rate allocations proportional to the user SE in both respective regions. The data rate of the kth user associated with ABS m can be expressed using

$$\mathcal{R}_k^m = \frac{W_{\Delta_v}}{K_v^m} \log_2\left(1 + \text{SINR}_{mk}\right), \quad (36)$$

where K_v^m is the user load of ABS m in one of the two regions (center or edge) with total ABS load $K^m = K_C^m + K_E^m$.

Another key metric to evaluate the overall network performance is the ASE, which is expressed in terms of bits/s/Hz/m^2. The ASE accounts for how efficiently the spectrum resources are exploited by the network within a certain area of interest. It can be expressed as [50]

$$ASE = \frac{\sum_{\forall m}\sum_{\forall k}\mathcal{R}_k^m}{\pi W_T R^2}. \quad (37)$$

Once the resource allocation is performed under the optimal cell partitions obtained by solving (32), we can determine the data rates of all the users to evaluate ASE of the network.

B. SIMULATION RESULTS AND DISCUSSION

We now present our remaining MATLAB-based numerical results using the above performance metrics assuming that the heights of all ABS cells in the proposed variable-height UAV-based network scheme are optimized as h_m^{opt}. An urban environment with a carrier frequency $f_c = 2$ GHz is considered, the key simulation parameters are listed in Table 1. The network is supposed to have a minimum and maximum number of ABSs of 7 and 25, respectively, due to practical constraints on resources availability, a maximum of 25 UAVs are assumed in the system. Note that the effect of interference was neglected for the height optimization, but it is applied to all simulations where applicable. Moreover, in order to exhibit the performance gains of the proposed UAV deployments with the aid of FFR, an equal bandwidth allocation policy is exerted for each cell under a widely used FFR policy ($\Psi = 0.5$). We adopt this approach to have a fair comparison and contrast with the equal-height UAV-based network, referred as $\mathcal{M}_{\text{E}}$ here. For brevity, we also refer to the proposed τ-tier variable-height network as $\mathcal{M}_{\text{V}}^{\tau}$.

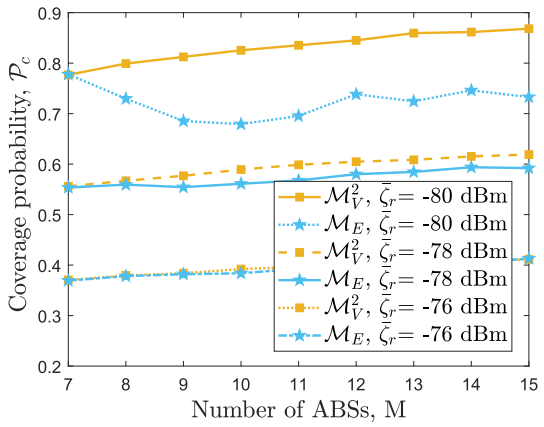

FIGURE 10. Coverage probability comparison of $\mathcal{M}_{\text{E}}$ and $\mathcal{M}_{\text{V}}^2$ models under different received power thresholds $\bar{\zeta}_r$ using directional antennas with optimized height $h_{m,D}^{opt}$, $\forall$ m $\in$ M.

Firstly, we show coverage probability $\mathcal{P}_c$ based performance using directional antennas in Figure 10. We used optimal height $h_{m,D}^{opt}$ of the ABS which corresponds to an optimal beamwidth obtained using (28). One can see that the $\mathcal{M}_{\text{V}}^2$ based deployments deliver distinctive coverage performance compared to the counterpart $\mathcal{M}_{\text{E}}$ model at different received power thresholds $\bar{\zeta}_r$ with an increasing number of ABSs M.

Moving to the omnidirectional antenna case, the results in Figure 11 show the SINR coverage probability comparison after the optimal resource partitioning under the FFR scheme. We can see substantial coverage gains for the $\mathcal{M}_{\text{V}}^2$ model compared to $\mathcal{M}_{\text{E}}$ for an increasing M under different SINR thresholds $\bar{\Omega}_s$. This gain partly comes from the increasing size of the coverage area under the central ABS which leverages from the frequency set $\mathcal{F}_2$ in the edge region (i.e., high SNR). That is, as M increases more users are encapsulated and

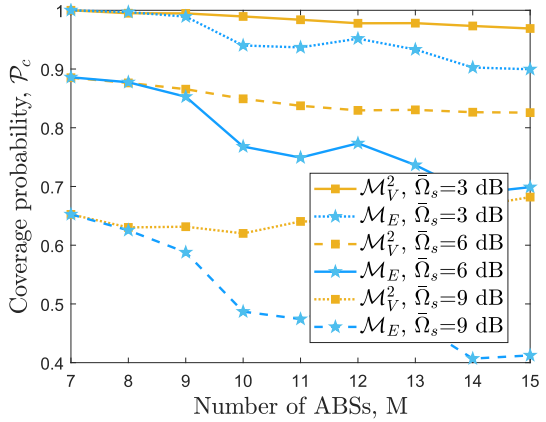

FIGURE 11. Coverage probability comparison of $\mathcal{M}_{\mathrm{E}}$ and $\mathcal{M}_{\mathrm{V}}^2$ under different SINR thresholds $\bar{\Omega}_s$ after optimizing the cell partition thresholds $\hat{\Omega}_{th}^m$ for all the ABS cells.

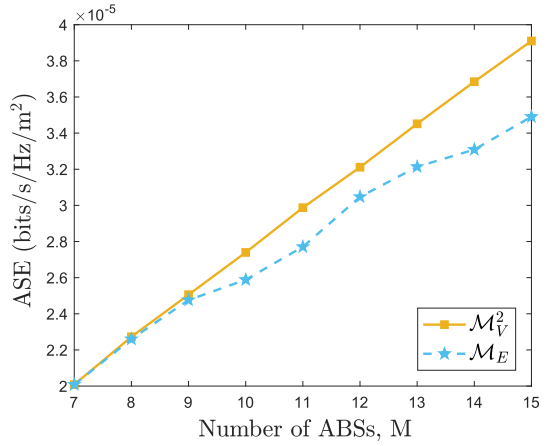

FIGURE 12. Area spectral efficiency (ASE) comparison of $\mathcal{M}_E$ and $\mathcal{M}_{\mathrm{V}}^2$ models after optimizing the cell partition thresholds $\hat{\Omega}_{th}^m$ for all the ABS cells.

benefit from an interference-free zone under the frequency set $\mathcal{F}_2$. Also, the average SINR level increases in the center region of the central ABS.

The ASE performance of the $\mathcal{M}_{\mathrm{V}}^2$ deployments is compared with the $\mathcal{M}_{\mathrm{E}}$ model in Figure 12. Clearly, the ASE gain for $\mathcal{M}_{\mathrm{V}}^2$ increases with M. It is worth mentioning that the bandwidth allocation to each user decreases in the central ABS as M is increased under the $\mathcal{M}_{\mathrm{V}}^2$ model. However, to some effect this problem is mitigated by the increasing SINRs of the central ABS. Importantly, the second tier users benefit from more bandwidth per user owing to the shrinking ABS cells. Moreover, the cell partition optimization makes a striking impact to cater the inflating interference emerging from the central ABS by pushing a balance of users in the center and edge regions to achieve an overall high ASE.

While the $\mathcal{M}_{\mathrm{V}}^2$ deployments show escalating coverage and ASE performance as M increases, it comes at the cost of an increasing disparity in the data rates of the users. Note that a user might be considered in outage (i.e., not satisfied) when a minimum required data rate is not achieved. One can observe from Figure 13 that the rate coverage R_c increases and then starts decreasing for different user rate threshold $\bar{\mathcal{R}}_{th}$. To this end, we can determine transition values for the number of UAVs for each $\bar{\mathcal{R}}_{th}$ beyond which the performance of the two-tier design in terms of rate coverage drops below the equal height benchmark scheme. That is, the transition from $\mathcal{M}_{\mathrm{V}}^2$ to $\mathcal{M}_{\mathrm{V}}^3$ (higher tier deployment presented in the next section) can be beneficial when the gain of two-tier design vanishes against the equal height design. For instance, in cases $\bar{\mathcal{R}}_{th} = 0.5$ Mbps and $\bar{\mathcal{R}}_{th} = 1$ Mbps, this transition is executed beyond $M = 12$ as the rate coverage R_c drops below its counterpart as observed in Figure 13. To gain more insight, rate coverage performance using different rate thresholds are plotted. It can be observed that the $\mathcal{M}_{\mathrm{V}}^2$ model exhibits better rate coverage gain compared to $\mathcal{M}_{\mathrm{E}}$ for the high rate threshold (i.e., 1.5 Mbps) even beyond $M = 12$. In fact, under this proposed systematic approach we leverage from the FFR assisted two-tier ABS deployment to achieve excellent coverage and ASE performance over $\mathcal{M}_{\mathrm{E}}$.

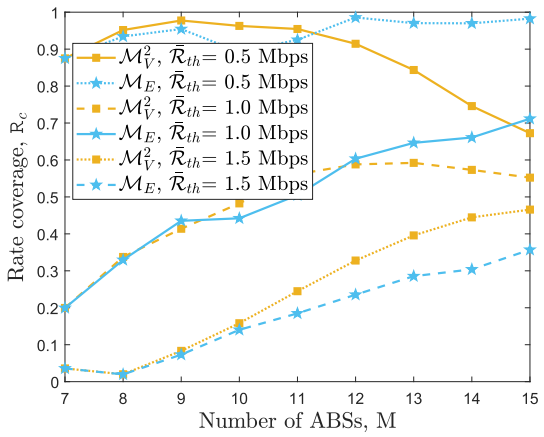

FIGURE 13. Rate coverage comparison of $\mathcal{M}_{\mathrm{E}}$ and $\mathcal{M}_{\mathrm{V}}^2$ models under different data rate thresholds $\bar{\mathcal{R}}_{th}$ for an increasing number of ABSs M.

VII. EXTENSION TO HIGHER TIERS

Our proposed approach for variable-height UAV network discussed in detail and demonstrated for the two-tier model in the previous sections can be readily extended to higher tiers. The proposed approach starts with the cell formation design for the UAV network determining the position and the radius of individual cells covered by UAV-based ABSs. Then the height of UAVs are optimized for each cell considering their radius and finally an FFR scheme is developed to mitigate ICI while maximizing throughput.

We first discuss the extension of two-tier cell formation problem to higher tiers using a recursive approach where the position and radius of individual UAVs are determined starting from the most outer tier (i.e., τth tier) down to the 2nd tier as summarized in Algorithm 3. In each step a two-tier cell formation design is developed based on Algorithm 1 introduced in section III to determine the cell formation

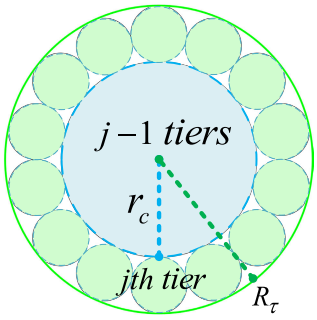

FIGURE 14. Cell formation design of *j*th tier using the two-tier model.

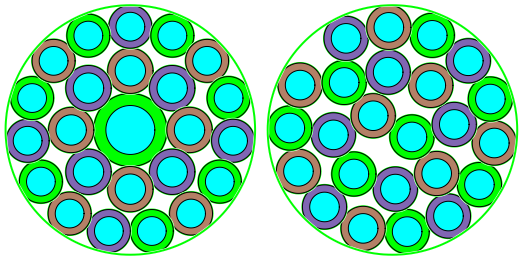

FIGURE 15. An illustration of FFR based resource allocation for ABS deployments $M = 24$, models $\mathcal{M}_{\mathrm{V}}^3$ (left) and $\mathcal{M}_{\mathrm{E}}$ (right).

parameters of the *j*th tier as well as the boundary of the $(j-1)$th tier as shown in Figure 14. To run the algorithm one, we require the boundary of the *j*th tier (as determined in the previous step) as well as the number of the UAVs allocated to that tier. Hence, we need to run this recursive approach in multiple iterations for all the possible combinations of UAV distribution among different tiers as indicated in Algorithm 3 and choose the optimal solution based on the distribution that provides the best performance. The objective function for choosing the best solution among different possible combinations of distributing UAVs within tiers is considered as

$$\Upsilon = \left(\sum_{m=1}^{M} \pi r_m^2\right) - \psi \chi_o, \tag{38}$$

where the first term in (38) represents the coverage maximization and the second term is introduced to limit the power consumption disparity between the UAVs in different tiers, which in turn leads to improved coverage lifetime. To address the power consumption disparity among variable-height UAVs, we already assumed that the network employs a more resourceful central UAV with coordination capability in the first tier while it has a set of homogeneous $(M-1)$ UAVs for the second and higher tier deployments. However, when the number of tiers $\tau > 2$, we need to limit power consumption of identical UAVs operating at different heights across different tiers. Note that $\psi \in \{0, 1\}$ where $\psi = 0$ transforms the objective function for purely coverage maximization considered for the two-tier design. We define $\chi_o = \frac{1}{\tau}\sum_{j=3}^{\tau} |\zeta_{t_2} - \zeta_{t_j}|$, where ζ_{t_2} and ζ_{t_j} are the total transmit power of ABSs operating in tier-2 and tier-*j*, respectively. The power consumption in different tiers are calculated based on (29) after height optimization for each cell as discussed in section V. Note that the height optimization step of our proposed network design only depends on the radius of the individual cells and therefore does not need any modifications for higher tiers.

The following expression is modelled to visualize the number of possible combinations $\mathcal{K}$ for a given set of ABS M and number of tiers τ as

$$\mathcal{K} = \frac{1}{2}\Big((\tau-3)(M-3\tau+2)^2 + (\tau-1)(M-3\tau+2)+2\Big), \quad \forall M \geqslant (3\tau-2). \tag{39}$$

Note that in order for Algorithm 3 to converge, the condition $M \geq (3\tau-2)$ should be satisfied, otherwise the solution will be infeasible i.e., violating the tangency rule. One can observe from (39) that the value of $\mathcal{K}$ depends on both M and τ, hence the complexity of Algorithm 3 is $\mathcal{O}\left(\frac{\tau(M-3\tau)^2}{2}\right)$.

The final step of our network design is the FFR-based scheme. Note that similar to height optimization, the development of FFR scheme including the SINR threshold optimization can be performed based on the same principles introduced in section V. An example of cell topology and FFR based resource configuration is illustrated in Figure 15 at $M = 24$ for both proposed $\mathcal{M}_{\mathrm{V}}^3$ and the benchmark $\mathcal{M}_{\mathrm{E}}$ models on the left and right side, respectively. It is worth mentioning that the cell edge frequency of the central ABS ($\mathcal{F}_2$ in $\mathcal{M}_{\mathrm{V}}^3$) can be reused in the third (or higher) tiers which offers an additional flexibility from the frequency allocation viewpoint.

In Figure 16, we present the coverage density of the equal-size, two-tier, and three-tier models $\mathcal{M}_{\mathrm{E}}$, $\mathcal{M}_{\mathrm{V}}^2$, and $\mathcal{M}_{\mathrm{V}}^3$, respectively, for an increasing number of ABSs M. It is evident that the coverage of $\mathcal{M}_{\mathrm{V}}^2$ is superior with an increasing margin while both $\mathcal{M}_{\mathrm{V}}^2$ and $\mathcal{M}_{\mathrm{V}}^3$ outperform the counterpart $\mathcal{M}_{\mathrm{E}}$ model. Note that the ratio of the area covered to the total area of the coverage region is known as the coverage density as in (13), which closely indicate the coverage probability of the network if directional antennas are employed. This is because the users outside the coverage footprint (main-lobe of the directional antenna) are either entirely ignored or they might receive a very insignificant service (i.e., very low SNR) from the side-lobes. For instance, if we consider 10 ABSs and employ directional antennas, even for a very low SNR value almost 24%, 9%, and 17% of the users will still remain uncovered under the $\mathcal{M}_{\mathrm{E}}$, $\mathcal{M}_{\mathrm{V}}^2$, and $\mathcal{M}_{\mathrm{V}}^3$ models, respectively. This strongly advocates for exploiting omnidirectional antennas over the directional antennas to improve the overall network throughput and user QoS.

The comparison between the two variants of the objective function in (38) for the $\mathcal{M}_{\mathrm{V}}^3$ model (i.e., $\psi \in \{0, 1\}$) is shown in Figure 17. It can be noticed that a substantial difference exists in the power consumption of the second and third tier ABSs, which is associated with the difference in the coverage lifetimes, with weight factor $\psi = 0$ (when the transmit power of the ABSs across the tiers is not comparable), while it

Algorithm 3 Recursive τ-Tier UAV Cellular Design

Input : Coverage area radius, R
Number of ABSs, M
Output: Horizontal locations of ABSs: $\hat{H}_m$, $(\forall\, 1 \leq m \leq M)$,
Cell radius for all tiers: $\hat{r}_j$, $(\forall\, 1 \leq j \leq \tau)$
initialize;
$\psi \leftarrow (0, 1)$, $\theta_r = \pi/2$
Set $\mathcal{K}$ as the number of possible combinations of distributing M UAVs into τ tiers.
for $i \leftarrow 1$ *to* $\mathcal{K}$ **do**
  Set the number of ABSs for each tier M_j, $(\forall\, 1 \leq j \leq \tau)$, based on the ith combination
  Set $R_\tau = R$
  for $j \leftarrow \tau$ *to* 2 **do**
    Run **Algorithm 1** with inputs R_j as coverage area radius and M_j as number of ABSs
    Set horizontal locations of ABSs in tier j as H_m and $R_{j-1} = r_c$ and $r_j(i) = r_e$ where H_m, r_c and r_e are outputs of **Algorithm 1**.
  end
  $r_1(i) = R_1\ \Upsilon(i) = \pi \left(\sum_{j=1}^{\tau} M_j r_j^2\right) - \psi\, \chi_o$
end
$\hat{\Upsilon} \leftarrow \max\,(\Upsilon(i))\,|_{i=1}^{\mathcal{K}}$
$\hat{H}_m \leftarrow \max\,(H_m(i))\,|_{i=1}^{\mathcal{K}}$
$\hat{r}_j \leftarrow \max\,(r_j(i))\,|_{i=1}^{\mathcal{K}}$
return $\hat{\Upsilon}$, $\hat{H}_m$ and $\hat{r}_j$ as the feasible solution for (38)

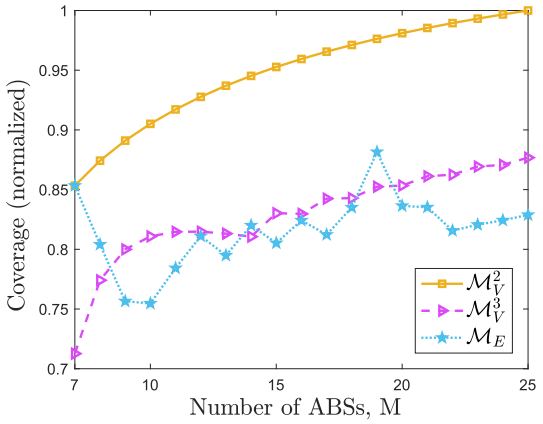

FIGURE 16. Coverage density (normalized) of UAV based network considering $\mathcal{M}_{\mathbf{E}}$, $\mathcal{M}_{\mathbf{V}}^{\mathbf{2}}$, and $\mathcal{M}_{\mathbf{V}}^{\mathbf{3}}$ models.

almost goes to zero for $\psi = 1$. On the other hand, coverage results are still very comparable for the two cases. Consequently, in order to avoid power consumption disparity while preserving good coverage, we are encouraged to deploy ABSs under the $\mathcal{M}_{\mathrm{V}}^3$ model using $\psi = 1$.

Next, we present some simulation results for the performance of $\mathcal{M}_{\mathrm{V}}^3$ as a representative of high-tier cellular design

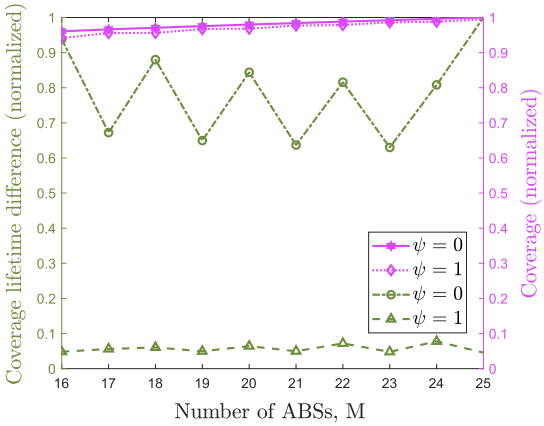

FIGURE 17. Total coverage and coverage lifetime difference of the second and third tier ABSs under the $\mathcal{M}_{\mathbf{V}}^{\mathbf{3}}$ model with two values of ψ.

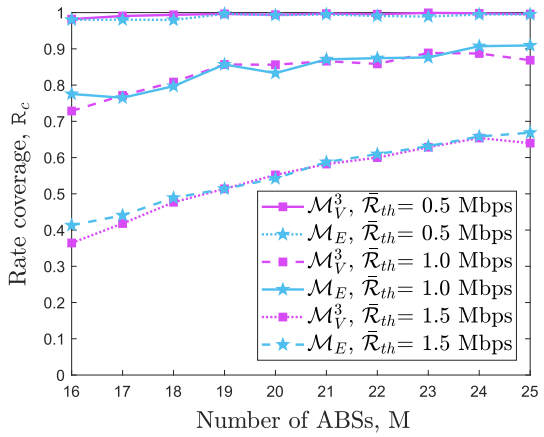

FIGURE 18. Rate coverage comparison of $\mathcal{M}_{\mathbf{E}}$ and $\mathcal{M}_{\mathbf{V}}^{\mathbf{3}}$ models under different data rate thresholds $\bar{\mathcal{R}}_{\boldsymbol{th}}$ for an increasing number of ABSs $\boldsymbol{M}$.

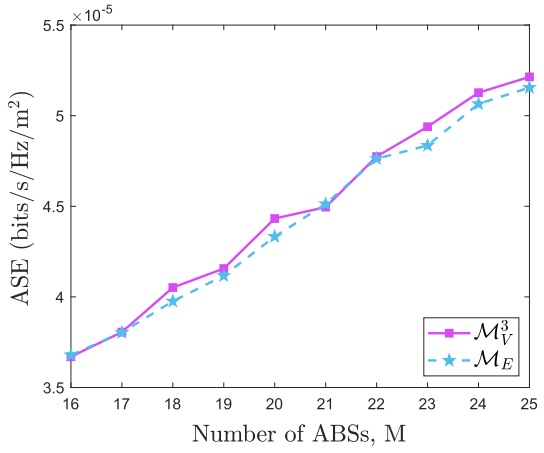

FIGURE 19. Area spectral efficiency (ASE) comparison of $\mathcal{M}_{\mathbf{E}}$ and $\mathcal{M}_{\mathbf{V}}^{\mathbf{3}}$ models after optimizing the cell partition thresholds $\hat{\Omega}_{\boldsymbol{th}}^{\boldsymbol{m}}$ for all the ABS cells.

in comparison to the benchmark scheme $\mathcal{M}_{\mathrm{E}}$. Figure 18 shows that, unlike the two-tier scheme, the rate coverage of $\mathcal{M}_{\mathrm{V}}^3$ does not drop below that of $\mathcal{M}_{\mathrm{E}}$ at different thresholds,

even with a larger number of UAVs. This is owing to the fact that $\mathcal{M}_{\mathrm{V}}^{3}$ reduces the large cell-size and transmit power disparity across the tiers that resulted in the large variation of user data rates under $\mathcal{M}_{\mathrm{V}}^{2}$, which justifies the transition to a higher-tier design for a larger number of UAVs.

The results in Figure 19 show that $\mathcal{M}_{\mathrm{V}}^{3}$ also exhibits marginally better or at least equal levels of ASE performance compared to the $\mathcal{M}_{\mathrm{E}}$ design. Therefore, it is evident that the proposed FFR-aided multi-tier network, which carries out a transition from two-tier to multi-tiers based on a performance metric (i.e., R_c), can always deliver better coverage and throughput performance compared to the equal height cellular design. Nevertheless, the performance of higher-tier variable height designs converges to the performance of the equal height design for larger number of UAVs as the optimal variable height model would converge to almost equal height model.

VIII. CONCLUSION

In this paper, we have proposed multi-UAV deployment techniques with the aid of circle packing to provide optimal coverage and throughput performance. We have shown a low-complexity, tractable, and efficient approach to adaptively increase or decrease the number of UAVs. A simple UAV height optimization method is proposed which shows superior outage performance and is also more energy-efficient compared to the most commonly used height optimization technique in the literature. The results clearly indicate that we can achieve considerable coverage and throughput (i.e., ASE) gains compared to the equal height UAV-based network by leveraging FFR and optimizing the cell partitions using the same system parameters. We have also proposed a low-complexity algorithm to switch from two-tier to higher-tier networks if certain QoS criterion (i.e., rate coverage) for a set of UAVs is not achieved. The proposed multi-tier network also exhibits better coverage performance while it shows slightly better or at least comparable levels of throughput and rate coverage performance. In essence, the proposed deployment method not only performs better under several widely used performance metrics but it can also easily handle failures or changes to the UAV network compared to the state-of-the-art model. This work could be extended to explore the effects of mobility under a circular trajectory of multiple UAVs across multiple-tiers with or without incorporating FFR. A multi-dimensional search for the ideal number of UAVs with optimal speed and separation distances can be used to assess the coverage and throughput performance of many UAVs in this scheme. Also, the impact of UAV stability on highly directional backhaul links could be a promising direction to pursue.

REFERENCES

[1] H. Shakhatreh, A. H. Sawalmeh, A. Al-Fuqaha, Z. Dou, E. Almaita, I. Khalil, N. S. Othman, A. Khreishah, and M. Guizani, "Unmanned aerial vehicles (UAVs): A survey on civil applications and key research challenges," *IEEE Access*, vol. 7, pp. 48572–48634, 2019.

[2] M. Y. Arafat, S. Poudel, and S. Moh, "Medium access control protocols for flying ad hoc networks: A review," *IEEE Sensors J.*, vol. 21, no. 4, pp. 4097–4121, Feb. 2021.

[3] L. Gupta, R. Jain, and G. Vaszkun, "Survey of important issues in UAV communication networks," *IEEE Commun. Surveys Tuts.*, vol. 18, no. 2, pp. 1123–1152, 2nd Quart., 2016.

[4] Y. Zeng, R. Zhang, and T. J. Lim, "Wireless communications with unmanned aerial vehicles: Opportunities and challenges," *IEEE Commun. Mag.*, vol. 54, no. 5, pp. 36–42, May 2016.

[5] M. Mozaffari, W. Saad, M. Bennis, and M. Debbah, "Efficient deployment of multiple unmanned aerial vehicles for optimal wireless coverage," *IEEE Commun. Lett.*, vol. 20, no. 8, pp. 1647–1650, Aug. 2016.

[6] X. Zhong, Y. Guo, N. Li, Y. Chen, and S. Li, "Deployment optimization of UAV relay for malfunctioning base station: Model-free approaches," *IEEE Trans. Veh. Technol.*, vol. 68, no. 12, pp. 11971–11984, Dec. 2019.

[7] J. Sun and C. Masouros, "Deployment strategies of multiple aerial BSs for user coverage and power efficiency maximization," *IEEE Trans. Commun.*, vol. 67, no. 4, pp. 2981–2994, Apr. 2019.

[8] M. Y. Arafat and S. Moh, "A Q-learning-based topology-aware routing protocol for flying ad hoc networks," *IEEE Internet Things J.*, early access, Jun. 16, 2021, doi: 10.1109/JIOT.2021.3089759.

[9] W. Khawaja, I. Guvenc, D. W. Matolak, U.-C. Fiebig, and N. Schneckenburger, "A survey of air-to-ground propagation channel modeling for unmanned aerial vehicles," *IEEE Commun. Surveys Tuts.*, vol. 21, no. 3, pp. 2361–2391, 3rd Quart., 2019.

[10] J. Urama, R. Wiren, O. Galinina, J. Kauppi, K. Hiltunen, J. Erkkila, F. Chernogorov, P. Etelaaho, M. Heikkila, J. Torsner, S. Andreev, and M. Valkama, "UAV-aided interference assessment for private 5G NR deployments: Challenges and solutions," *IEEE Commun. Mag.*, vol. 58, no. 8, pp. 89–95, Aug. 2020.

[11] O. S. Oubbati, M. Atiquzzaman, T. A. Ahanger, and A. Ibrahim, "Softwarization of UAV networks: A survey of applications and future trends," *IEEE Access*, vol. 8, pp. 98073–98125, 2020.

[12] A. Al-Hourani, S. Kandeepan, and S. Lardner, "Optimal LAP altitude for maximum coverage," *IEEE Wireless Commun. Lett.*, vol. 3, no. 6, pp. 569–572, Dec. 2014.

[13] H. Niu, X. Zhao, and J. Li, "3D location and resource allocation optimization for UAV-enabled emergency networks under statistical QoS constraint," *IEEE Access*, vol. 9, pp. 41566–41576, 2021.

[14] S.-Y. Park, C. S. Shin, D. Jeong, and H. Lee, "DroneNetX: Network reconstruction through connectivity probing and relay deployment by multiple UAVs in ad hoc networks," *IEEE Trans. Veh. Technol.*, vol. 67, no. 11, pp. 11192–11207, Nov. 2018.

[15] S. K. Singh, K. Agrawal, K. Singh, C.-P. Li, and W.-J. Huang, "On UAV selection and position-based throughput maximization in multi-UAV relaying networks," *IEEE Access*, vol. 8, pp. 144039–144050, 2020.

[16] A. A. Khuwaja, G. Zheng, Y. Chen, and W. Feng, "Optimum deployment of multiple UAVs for coverage area maximization in the presence of co-channel interference," *IEEE Access*, vol. 7, pp. 85203–85212, 2019.

[17] N. Namvar, A. Homaifar, A. Karimoddini, and B. Maham, "Heterogeneous UAV cells: An effective resource allocation scheme for maximum coverage performance," *IEEE Access*, vol. 7, pp. 164708–164719, 2019.

[18] M. A. Ali and A. Jamalipour, "UAV-aided cellular operation by user offloading," *IEEE Internet Things J.*, vol. 8, no. 12, pp. 9855–9864, Jun. 2021.

[19] P. Yang, X. Cao, C. Yin, Z. Xiao, X. Xi, and D. Wu, "Proactive drone-cell deployment: Overload relief for a cellular network under flash crowd traffic," *IEEE Trans. Intell. Transp. Syst.*, vol. 18, no. 10, pp. 2877–2892, Oct. 2017.

[20] H. N. Qureshi and A. Imran, "On the tradeoffs between coverage radius, altitude, and beamwidth for practical UAV deployments," *IEEE Trans. Aerosp. Electron. Syst.*, vol. 55, no. 6, pp. 2805–2821, Dec. 2019.

[21] X. Li, D. Guo, H. Yin, and G. Wei, "Drone-assisted public safety wireless broadband network," in *Proc. IEEE Wireless Commun. Netw. Conf. Workshops (WCNCW)*, Mar. 2015, pp. 323–328.

[22] C. Shen, T.-H. Chang, J. Gong, Y. Zeng, and R. Zhang, "Multi-UAV interference coordination via joint trajectory and power control," *IEEE Trans. Signal Process.*, vol. 68, pp. 843–858, 2020.

[23] J. Lyu, Y. Zeng, R. Zhang, and T. J. Lim, "Placement optimization of UAV-mounted mobile base stations," *IEEE Commun. Lett.*, vol. 21, no. 3, pp. 604–607, Mar. 2017.

[24] A. H. Arani, P. Hu, and Y. Zhu, "Fairness-aware link optimization for space-terrestrial integrated networks: A reinforcement learning framework," *IEEE Access*, vol. 9, pp. 77624–77636, 2021.

[25] T. M. Ho, K.-K. Nguyen, and M. Cheriet, "UAV control for wireless service provisioning in critical demand areas: A deep reinforcement learning approach," *IEEE Trans. Veh. Technol.*, vol. 70, no. 7, pp. 7138–7152, Jul. 2021.

[26] Q. Wu, Y. Zeng, and R. Zhang, "Joint trajectory and communication design for multi-UAV enabled wireless networks," *IEEE Trans. Wireless Commun.*, vol. 17, no. 3, pp. 2109–2121, Mar. 2018.

[27] M. Alzenad, A. El-Keyi, F. Lagum, and H. Yanikomeroglu, "3-D placement of an unmanned aerial vehicle base station (UAV-BS) for energy-efficient maximal coverage," *IEEE Wireless Commun. Lett.*, vol. 6, no. 4, pp. 434–437, Aug. 2017.

[28] H. Shakhatreh, A. Khreishah, N. S. Othman, and A. Sawalmeh, "Maximizing indoor wireless coverage using UAVs equipped with directional antennas," in *Proc. IEEE 13th Malaysia Int. Conf. Commun. (MICC)*, Nov. 2017, pp. 175–180.

[29] H. Shakhatreh, A. Khreishah, and I. Khalil, "Indoor mobile coverage problem using UAVs," *IEEE Syst. J.*, vol. 12, no. 4, pp. 3837–3848, Dec. 2018.

[30] F. Gao, Y. Zhou, X. Ma, T. Yang, N. Cheng, and N. Lu, "Coverage-maximization and energy-efficient drone small cell deployment in aerial-ground collaborative vehicular networks," in *Proc. IEEE 4th Int. Conf. Comput. Commun. Syst. (ICCCS)*, Feb. 2019, pp. 559–564.

[31] M. M. Azari, F. Rosas, K.-C. Chen, and S. Pollin, "Ultra reliable UAV communication using altitude and cooperation diversity," *IEEE Trans. Commun.*, vol. 66, no. 1, pp. 330–344, Jan. 2018.

[32] H. Zhang, S. Chen, L. Feng, Y. Xie, and L. Hanzo, "A universal approach to coverage probability and throughput analysis for cellular networks," *IEEE Trans. Veh. Technol.*, vol. 64, no. 9, pp. 4245–4256, Sep. 2015.

[33] M. Mozaffari, W. Saad, M. Bennis, and M. Debbah, "Mobile unmanned aerial vehicles (UAVs) for energy-efficient Internet of Things communications," *IEEE Trans. Wireless Commun.*, vol. 16, no. 11, pp. 7574–7589, Nov. 2017.

[34] H. Zhao, H. Wang, W. Wu, and J. Wei, "Deployment algorithms for UAV airborne networks toward on-demand coverage," *IEEE J. Sel. Areas Commun.*, vol. 36, no. 9, pp. 2015–2031, Sep. 2018.

[35] G. Yang, R. Dai, and Y. C. Liang, "Energy-efficient UAV backscatter communication with joint trajectory design and resource optimization," *IEEE Trans. Wireless Commun.*, vol. 20, no. 2, pp. 926–941, Oct. 2021.

[36] Z. Yang, C. Pan, M. Shikh-Bahaei, W. Xu, M. Chen, M. Elkashlan, and A. Nallanathan, "Joint altitude, beamwidth, location, and bandwidth optimization for UAV-enabled communications," *IEEE Commun. Lett.*, vol. 22, no. 8, pp. 1716–1719, Aug. 2018.

[37] S. Ahmed, M. Z. Chowdhury, and Y. M. Jang, "Energy-efficient UAV-to-user scheduling to maximize throughput in wireless networks," *IEEE Access*, vol. 8, pp. 21215–21225, 2020.

[38] Z. Gáspár and T. Tarnai, "Upper bound of density for packing of equal circles in special domains in the plane," *Periodica Polytech. Civil Eng.*, vol. 44, no. 1, pp. 13–32, 2000.

[39] E. Kalantari, H. Yanikomeroglu, and A. Yongacoglu, "On the number and 3D placement of drone base stations in wireless cellular networks," in *Proc. IEEE 84th Veh. Technol. Conf. (VTC-Fall)*, Sep. 2016, pp. 1–6.

[40] A. Fotouhi, M. Ding, and M. Hassan, "Flying drone base stations for macro hotspots," *IEEE Access*, vol. 6, pp. 19530–19539, 2018.

[41] K. Gokcesu and S. S. Kozat, "An online minimax optimal algorithm for adversarial multiarmed bandit problem," *IEEE Trans. Neural Netw. Learn. Syst.*, vol. 29, no. 11, pp. 5565–5580, Nov. 2018.

[42] Y. Xu, A. Anpalagan, Q. Wu, L. Shen, Z. Gao, and J. Wang, "Decision-theoretic distributed channel selection for opportunistic spectrum access: Strategies, challenges and solutions," *IEEE Commun. Surveys Tuts.*, vol. 15, no. 4, pp. 1689–1713, 4th Quart., 2013.

[43] G. Geraci, A. G. Rodriguez, L. G. Giordano, D. López-Pérez, and E. Björnson, "Understanding UAV cellular communications: From existing networks to massive MIMO," *IEEE Access*, vol. 6, pp. 67853–67865, 2018.

[44] S.-H. Chang, H.-G. Park, S.-H. Kim, and J. P. Choi, "Study on coverage of full frequency reuse in FFR systems based on outage probability," *IEEE Trans. Commun.*, vol. 66, no. 11, pp. 5828–5843, Nov. 2018.

[45] S. Kumar, S. Kalyani, L. Hanzo, and K. Giridhar, "Coverage probability and achievable rate analysis of FFR-aided multi-user OFDM-based MIMO and SIMO systems," *IEEE Trans. Commun.*, vol. 63, no. 10, pp. 3869–3881, Oct. 2015.

[46] J. García-Morales, G. Femenias, and F. Riera-Palou, "On the design of OFDMA-based FFR-aided irregular cellular networks with shadowing," *IEEE Access*, vol. 6, pp. 7641–7653, 2018.

[47] C. Raiman and J. Posluszny, "Sectorized omnidirectional antenna," U.S. Patent 10 107 615, Oct. 2, 2003.

[48] A. Ghosh, J. Zhang, J. G. Andrews, and R. Muhamed, *Fundamentals of LTE*. London, U.K.: Pearson, 2010.

[49] H.-B. Chang and I. Rubin, "Optimal downlink and uplink fractional frequency reuse in cellular wireless networks," *IEEE Trans. Veh. Technol.*, vol. 65, no. 4, pp. 2295–2308, Apr. 2016.

[50] G. Miao and G. Song, *Energy and Spectrum Efficient Wireless Network Design*. Cambridge, U.K.: Cambridge Univ. Press, 2014.

MUHAMMAD NAFEES (Member, IEEE) received the B.S. degree in computer engineering from COMSATS University Islamabad, Lahore Campus, Pakistan, in 2008, and the M.Sc. degree in wireless networks from Queen Mary University of London, U.K., in 2010. He is currently pursuing the Ph.D. degree in electrical engineering with the School of Engineering, Institute for Digital Communication, The University of Edinburgh, U.K. From 2011 to 2018, he served as a Lecturer for the Department of Electrical and Computer Engineering, COMSATS University Islamabad, Lahore Campus. He joined the School of Engineering, Institute for Digital Communication, The University of Edinburgh, in October 2018. His research interests include unmanned aerial vehicles (UAVs), fifth-generation and beyond (5GB) communications, hybrid RF/optical communications, game theory, and machine learning for wireless networks.

JOHN THOMPSON (Fellow, IEEE) is currently a Professor with the School of Engineering, The University of Edinburgh. He also specializes in antenna array processing, cooperative communications systems, and energy-efficient wireless communications. He has published in excess of 350 articles on these topics. He was a Coordinator for the recently completed EU Marie Curie Training Network Advantage, which studies how communications and power engineering can provide future smart grid systems. He also participates in several projects which study new concepts for future generation wireless communications. In January 2016, he was elevated to fellow of the IEEE for research contributions to antenna arrays and multihop communications. In 2018, he was the Co-Chair of the IEEE SmartGridComm Conference, Aalborg, Denmark.

MAJID SAFARI (Senior Member, IEEE) received the B.Sc. degree in electrical and computer engineering from the University of Tehran, Iran, in 2003, the M.Sc. degree in electrical engineering from Sharif University of Technology, Iran, in 2005, and the Ph.D. degree in electrical and computer engineering from the University of Waterloo, Canada, in 2011. He is currently a Reader with the Institute for Digital Communications, The University of Edinburgh. Before joining The University of Edinburgh, in 2013, he held Postdoctoral Fellowship at McMaster University, Canada. His main research interests include the application of information theory and signal processing in optical communications, including fiber-optic communication, free-space optical communication, visible light communication, and quantum communication. He was the TPC Co-Chair of the 4th International Workshop on Optical Wireless Communication, in 2015. He is also an Associate Editor of the IEEE TRANSACTIONS ON COMMUNICATIONS.